

Infrared spectra of neutral bent carbon dioxide

Sergy Yu. Grebenshchikov*

Department of Chemistry, Technical University of Munich,

Lichtenbergstr. 4, 85747 Garching, Germany

A combined ab initio and quantum dynamical study characterizes a family of bent neutral carbon dioxide molecules in terms of their vibrational levels, electric dipole moment surfaces, and infrared spectra in the gas phase. The considered isomers include the dioxiranylidene (cyclic) form of CO₂ with the equilibrium valence angle of 72°, belonging to the ground electronic state, and four open structures with the valence angles of 118°/119° (belonging to the singlet and triplet electronic states 2¹A' and 1³A', respectively) and 127°/128° (states 1¹A'' and 1³A'', respectively). All studied bent structures possess permanent dipole moments. For all isomers, the antisymmetric stretch fundamental is the strongest infrared transition. Individual bent molecules can be distinguished on the basis of strong absorption bands in the frequency window 1100 cm⁻¹ — 1800 cm⁻¹ as well as isotopic shifts in the progression of antisymmetric stretch mode. Excitation of bent neutral carbon dioxide near a perfect metal surface is also briefly discussed. It is argued that the excitation energy from the linear ground state exhibits a red red shift which depends on the molecule—metal distance.

I. INTRODUCTION

This paper explores the spectroscopic properties of bent configurations of neutral CO₂ in the low lying electronically excited singlet and triplet states with the equilibrium bending angles lying in the range of $70^\circ \leq \alpha_{\text{OCO}} \leq 130^\circ$. The focus is on the dipole moment functions and the vibrational infrared (IR) spectra. The analysis is performed using a combination of a high level electronic structure theory and quantum dynamics.

Figure 1(a) gives an overview of the low energy portion of the experimental vacuum ultraviolet (UV) absorption spectrum of CO₂ consisting of two weak well separated bands.¹

* Email: Sergy.Grebenshchikov@ch.tum.de

In a recent *ab initio* quantum mechanical study, these bands were accurately reproduced and the diffuse absorption lines were assigned in terms of the principal vibrational modes of the molecule trapped in the unstable resonance states [shown as a stick spectrum in panel (a)].² The high energy band is mainly due to pseudorotational motion in the plane of the two CO bonds, while the low energy band is dominated by the bending progressions.^{2,3} These assignments are schematically illustrated in Fig. 1(a). The present study originates from the observation that several lines near $65\,000\text{ cm}^{-1}$ stem from the ‘cyclic’ OCO molecule, known as dioxiranylidene, with the valence angle of $\alpha_{\text{OCO}} = 72^\circ$. The identification of this isomer in the absorption spectrum has several chemically significant implications because bent CO_2 molecules are characterized by enhanced reactivity; one speaks of activated carbon dioxide.

Activation of carbon dioxide is often considered a first step in the selective photoconversion of this inert greenhouse gas into value-added chemicals, such as fuels. The activation is commonly achieved photocatalytically, at a metal or metal oxide surface acting as a photosensitizer.^{4,5} The bent activated molecules in this case are anion radicals $\text{CO}_2^{\gamma-}$ — the key intermediates formed via a partial electron transfer from metal.^{6,7} The negative electron affinity of carbon dioxide makes a single electron transfer to the molecule non-spontaneous. This is a limitation of the photocatalytic approach which affects its efficiency and forces one to look for alternative activation and reduction schemes.

One such scheme is the activation/dissociation of the neutral CO_2 in the gas phase. Preheating of the gaseous carbon dioxide gradually shifts absorption from the vacuum UV range towards longer wavelengths at the UV edge of the solar spectrum making solar based activation feasible.^{8,9} Recent measurements and calculations report appreciable absorption of preheated CO_2 at wavelengths reaching 300 nm .^{10–12} The present study indicates that near metal surfaces comparable red shifts in the absorption can be realized even at ambient temperatures. Plasmolysis is another gas phase-based scheme of CO_2 -to-fuel conversion.^{13–15} Bent CO_2 species near dissociation threshold are believed to affect the inelastic electron excitation cross sections in plasma and to play the role of transient species enhancing the dissociation rates and the carbon monoxide yields.

Bent states of CO_2 have a long history of studies. It is well known that its low lying excited states, both singlets ($2^1A'$ and $1^1A''$) and triplets ($1^3A'$ and $1^3A''$), arising from the excitations into the $6a_1$ component of the lowest unoccupied $2\pi_u$ orbital, support bent equilibria as a direct consequence of the Walsh rules.^{6,16,17} Panel (b) of Fig. 1 provides an

overview of bent electronic states relevant for the present work. All states are labeled using the irreps of the C_s symmetry group even though the actual symmetry of the bent molecules is C_{2v} . The singlet and triplet states of A' symmetry have equilibrium angles of $118^\circ/119^\circ$; for the states of A'' symmetry, the equilibrium angles are $128^\circ/129^\circ$. For brevity, all bent equilibrium structures of carbon dioxide will hereafter be termed ‘isomers’. The OCO angle for the state $2^1A'$ (correlating at C_{2v} geometries with 1B_2) was predicted by Dixon in his seminal analysis of the CO flame emission bands.¹⁸ Three decades later, Cossart-Magos and co-workers³ detected two bending progressions in the wavelength range 172 nm—198 nm (photon energies between $51\,000\text{ cm}^{-1}$ and $57\,000\text{ cm}^{-1}$) which they assigned to the bent state $1^1A''$ excited in a perpendicular transition from \tilde{X} . The near-equilibrium shapes of the potential energy functions of the bent singlet and triplet states were investigated by Spielfiedel et al.¹⁶ at the CASSCF level of theory (complete active space self-consistent field method). Recently, the global potential energy surfaces of the six lowest singlet states of CO_2 were mapped out using the internally-contracted multireference configuration interaction singles and doubles (MRD-CI) method and a large atomic basis set.¹⁹ These calculations accurately reproduced the measured absorption spectrum and allowed definitive assignments of many diffuse spectral bands.² The UV absorption spectra of the bent triplet states were calculated by Schmidt et al.,²⁰ while the singlet-singlet and triplet-singlet emission spectra were recently analyzed in Ref. 21.

Despite numerous studies, a systematic spectroscopic analysis of the neutral bent isomers remains outstanding and their vibrational states are poorly understood. A case in point is dioxiranylidene, which was predicted by Feller et al.²² Its equilibrium geometry and the energetic stability were analyzed in Refs. 23 and 24. While its signature in the vacuum UV absorption spectrum has been identified,² the vibrational spectrum of cyclic CO_2 is practically unknown.

In this study I extend the previous work and present a detailed analysis of the dipole moment functions and the IR vibrational spectra of the five stable bent isomers of CO_2 in the low lying excited singlet and triplet electronic states. It is hoped that the predicted IR intensities and the isotope shifts, calculated for several isotopomers, can help experimental identification of the neutral activated carbon dioxide intermediates.

The paper is organized as follows: The ab initio calculations and the potential energy profiles along the bending angle are discussed in Sect. II together with the corresponding

dipole moment functions. Section III briefly characterizes the vibrational states of the bent isomers, compares their fundamental frequencies with the known values for the linear CO_2 and for the bent anion radical CO_2^- , and discusses the IR spectra for excitations out of the ground vibrational states in the bent equilibria. The isotope dependence of the IR spectra is illustrated for the singlet electronic states. Section IV concludes and discusses a possible extension of this study to include stabilization of the polar bent isomers near metal surfaces due to dipole-image dipole interactions.

II. STATIC PROPERTIES OF BENT ISOMERS OF CO_2

Three-dimensional potential energy surfaces (PESs) of the ground electronic state \tilde{X}^1A' and the bent singlet states $2A'$ and $1A''$ have been described in detail in Ref. 19. They were calculated using the MRD-CI method based on the CASSCF calculations with 16 electrons in 12 active orbitals and 6 electrons in three fully optimized closed-shell inner orbitals. The doubly augmented correlation consistent polarized valence quadrupole zeta (d-aug-cc-pVQZ) atomic basis set due to Dunning,²⁵ is used. All calculations were performed using the MOLPRO package.²⁶ The quality of the MRD-CI potential energy surfaces in the Franck-Condon (FC) zone has been discussed in Refs. 2 and 12. In the interaction region, the calculated PESs agree well with the potentials recently calculated at the coupled cluster (EOM-CCSD) level of theory.²⁷

Here, the calculations of Ref. 2 are improved in one respect: New points are added to the angular grid near $\alpha_{\text{OCO}} = 72^\circ$, 118° , and 127° , as well as in the range $30 \leq \alpha_{\text{OCO}} \leq 60^\circ$ (~ 500 geometries in total are additionally calculated) in order to improve the description of bent equilibria. Their characteristic features are summarized in Table I; the potential cuts along the minimum energy path are shown in Fig. 1(b). The cyclic isomer $\text{CO}_2(72^\circ|\tilde{X}^1A')$ in the adiabatic ground state \tilde{X}^1A' is C_{2v} symmetric, with two CO bond lengths of $2.51 a_0$ substantially elongated relative to the linear equilibrium of $\text{CO}_2(180^\circ|\tilde{X}^1A')$. It is separated from the global linear minimum by a ~ 0.45 eV high potential barrier at $\alpha_{\text{OCO}} = 90^\circ$.²⁸ The electronic origin of the cyclic minimum can be traced to the state $4^1A'$ [not shown in Fig. 1(b)] which at linear geometries becomes a component of the orbitally degenerate state $2^1\Delta'_u$ resulting from an electronic promotion from the molecular orbital $1\pi_u$ into the Rydberg-type orbital $3p\pi_u$.^{16,17,19} The other two singlet isomers $\text{CO}_2(118^\circ|2^1A')$ and $\text{CO}_2(127^\circ|1^1A'')$

are also C_{2v} symmetric (see Table I). These open structures have similar energies and are located ~ 0.5 eV below the cyclic minimum. All three bent equilibria in the singlet states lie below the threshold of the singlet dissociation channel $\text{CO}(\tilde{X}^1\Sigma^+) + \text{O}(^1D)$. The two open structures are also quasi-stable relative to the lower energy triplet dissociation channel $\text{CO}(\tilde{X}^1\Sigma^+) + \text{O}(^3P)$ (the potential minima practically coincide with the threshold energy). Note however that the spin-orbit coupling in CO_2 is weak, of the order of 80 cm^{-1} ,²⁷ and the rate of internal conversion into the triplet dissociation channel is expected to be small.

The triplet states $1^3A'$ and $1^3A''$ are calculated with the same atomic basis and at the same level of theory as the singlets. The calculations are performed on a three dimensional grid of internal molecular coordinates, with the CO bond distances ranging from $1.8 a_0$ to $5.0 a_0$, and the valence angle in the range $\alpha_{\text{OCO}} = [70^\circ, 175^\circ]$; energies for $\alpha_{\text{OCO}} < 70^\circ$ are extrapolated. The triplet potentials along the bending angle are compared with the singlets in Fig. 1(b). The states $1^3A'$ and $1^3A''$ have minima located at nearly the same angles as their singlet counterparts $2^1A'$ and $1^1A''$ [cf. Table I]. In each singlet/triplet pair of open isomers, the triplet one is more stable (by 0.50 eV for $2^1A'/1^3A'$ and by 0.19 eV for $1^1A''/1^3A''$). Both triplet states lie below the asymptote $\text{CO}(\tilde{X}^1\Sigma^+) + \text{O}(^3P)$.

The ab initio electric dipole moments in different electronic states are computed with MOLPRO at the MRD-CI level of theory using the same coordinate grid as for the PESs above. The molecular axes (x', y', z') in these calculations are chosen as in Ref. 19, i.e. x' is orthogonal to the molecular plane, z' runs along one of the CO bonds and $y' \perp z'$. The in-plane components of the electric dipole are generally non-zero, while the component along x' vanishes. For further analysis, the dipole moments are transformed to the bisector frame (x, y, z) , with $x = x'$, the axis z lying on a bisector of the α_{OCO} angle, and $y \perp z$. Values between the grid points are obtained by interpolation using cubic splines.

Cuts through the dipole moment surfaces $\mu_{y,z}(R_1, R_2, \alpha_{\text{OCO}})$ in the plane (R_1, R_2) of the two CO bond lengths are shown in Fig. 2(a,b,c) for the singlet states, and in Fig. 3(a,b) for the triplet states. The bending angle is fixed to the equilibrium value for the given bent state. The components of the dipole moments obey simple symmetry rules with respect to the interchange of the two CO bonds:

$$\begin{aligned} \mu_z(R_1, R_2) &= \mu_z(R_2, R_1) \\ \mu_y(R_1, R_2) &= -\mu_y(R_2, R_1); \end{aligned} \tag{1}$$

the component μ_y (irrep b_2) is antisymmetric and vanishes in C_{2v} -symmetric equilibria, while the component μ_z is symmetric (irrep a_1), so that the bent isomers possess permanent electric dipoles. The dipole moments at equilibrium, $\mu_z \equiv \mu_{\text{eq}}$, are given in Table I, and the corresponding dipole vectors are illustrated in Fig. 1(b). The dependence of μ_{eq} on the equilibrium bending angle is non-monotonic, with the largest dipole moment of 1 D found for $\alpha_{\text{OCO}} = 118^\circ$ for the singlet state $2^1A'$. The cyclic CO_2 has a dipole moment of -0.25 D. This is the only isomer, for which the direction of the μ_z vector, $\text{C}^{\delta-} \rightarrow \text{O}_2^{\delta}$, is opposite to what one would expect on the basis of the electronegativity. The sign reversion of the dipole moment function was studied by Harrison for carbon monoxide.²⁹ He demonstrated that the net sign of the dipole moment is determined by a trade off of the direct charge contribution and the induced atomic dipoles. The permanent dipoles of the triplet states are generally smaller than those of their twin singlet states, and the dipoles of all neutral bent isomers are comparable or larger than the dipole of the carbon dioxide anion CO_2^- .

While the permanent dipole moments characterize bent equilibria, the dependences of μ_y and μ_z on the displacements from the equilibrium geometry control the intensity patterns in the vibrational IR spectra. The reflection symmetry of the components, Eq. (1), is utilized in Figs. 2(a,b,c) and 3(a,b): In each panel, the antisymmetric function μ_y is shown above and the symmetric function μ_z is shown below the diagonal $R_1 = R_2$. Near the diagonal, the component μ_z grows linearly along the symmetric stretch coordinate $R_+ = (R_1 + R_2)/2$ and along the bending angle α_{OCO} ; the component μ_y grows linearly along the antisymmetric stretch coordinate $R_- = (R_1 - R_2)/2$. The slopes of these linear dependences are the coefficients of the Herzberg-Teller expansion for the dipole moments;³⁰ their absolute values are listed in Table I. Although $\mu_z \gg \mu_y$ for both singlet and triplet states in the FC zone, the weak component μ_y grows rapidly with R_- implying that an intense line of the antisymmetric stretch fundamental can be expected in the IR spectra. For two singlet isomers, $\text{CO}_2(72^\circ|X^1A')$ and $\text{CO}_2(118^\circ|2^1A')$, the components μ_y are monotonic functions of R_- . In contrast, the functions μ_y for the isomers $\text{CO}_2(127^\circ|X^1A'')$, $\text{CO}_2(119^\circ|1^3A')$, and $\text{CO}_2(128^\circ|1^3A'')$ develop pronounced maxima close to the diagonal line $R_1 = R_2$. For these isomers, higher derivatives of μ_y are expected to significantly contribute to the Herzberg-Teller expansion.

III. THE INFRARED SPECTRA OF BENT ISOMERS OF CO₂

The vibrational states of bent CO₂ isomers are calculated quantum mechanically using the program package ‘PolyWave’³¹ (see Appendix for the computational details).

The fundamental frequencies of the symmetric stretch (ω_s), bend (ω_b), and antisymmetric stretch (ω_a) vibrations are listed in Table I and compared with the known frequencies of the linear CO₂ and of the CO₂⁻ anion radical. The frequencies ω_s and ω_b only weakly depend on the equilibrium angle. The calculated bending frequencies lie between between 600 cm⁻¹ and 700 cm⁻¹; the symmetric stretch frequencies range from about 1300 cm⁻¹ to 1500 cm⁻¹ (an exception is the isomer CO₂(128°|1³A'') in which $\omega_s = 1088$ cm⁻¹ is rather low). However, the deviations relative to the linear molecule are sufficient to tune the frequencies ω_s and ω_b away from the anharmonic 1 : 2 Fermi resonance³² which dominates the vibrational spectrum of linear OCO. The calculations agree well with the experimental estimates³ available for the state 1¹A'' ($\omega_b \approx 600$ cm⁻¹ and $\omega_s \approx 1370$ cm⁻¹), as well as with the previous theoretical results. The frequency of the antisymmetric stretch mode undergoes the most conspicuous change and in the bent isomers substantially deviates from $\omega_a = 2349$ cm⁻¹ of the linear CO₂(180°|X¹A'). The authors of Ref. 16 came to the same conclusion using CASSCF method. The antisymmetric stretch frequency tends to decrease with decreasing equilibrium bending angle reaching the value of 683 cm⁻¹ in the cyclic CO₂(72°|X¹A'); in fact, ω_a and ω_b in this case become accidentally degenerate. Table I demonstrates that the dependence of ω_a on α_{OCO} is not simple and not monotonous. In particular, the antisymmetric stretch frequencies of the triplet states are different from those of the singlet states with the same equilibrium angle. Nevertheless, the frequency ω_a remains the most convenient proxy for the geometry of the activated CO₂. As discussed below, the antisymmetric stretch fundamental is the strongest transition in the IR spectra of bent CO₂.

Anharmonic couplings between vibrational modes in bent isomers are generally weak. Many vibrational eigenfunctions $\psi_{\mathbf{n}}$ have unperturbed nodal lines and can be assigned quantum numbers v_s , v_b , and v_a corresponding to the symmetric stretch, bend, and antisymmetric stretch modes, respectively ($\mathbf{n} = (v_s, v_b, v_a)$ is a vector index). Table II in the Appendix summarizes the assigned vibrational states with energies up to 5000 cm⁻¹ above the ground vibrational level. The potential wells for different isomers have different depths (see Table I) and support different numbers of bound states. The longest lists

of assignable states are found for the bent molecules $\text{CO}_2(118^\circ|2^1A')$, $\text{CO}_2(127^\circ|1^1A'')$, and $\text{CO}_2(119^\circ|1^3A')$; for them, the potential wells are deep, 2 eV for the two singlet species, and 1.2 eV for the triplet one. The potential wells of the remaining two isomers are rather shallow. For $\text{CO}_2(72^\circ|\tilde{X}^1A')$, only the vibrational levels with energies below the ~ 0.45 eV high potential barrier, separating the cyclic minimum from the region of $\alpha_{\text{OCO}} > 90^\circ$, are included (states localized in the cyclic well and belonging to the pure bending progression can also be found at higher energies, even 1.5 eV above the barrier top²). The well of the triplet carbon dioxide $\text{CO}_2(128^\circ|1^3A'')$ is separated from the dissociation channel by a potential barrier which in the present MRD-CI calculations lies 0.56 eV above minimum (the authors of of Ref. 16 reported this state, calculated using CASSCF method, as unbound). Note however, that only short vibrational progressions are found in the IR spectra discussed below, and even moderately excited vibrational states with the quantum numbers larger than 3 or 4 do not show up in the spectra.

For each isomer, the IR intensities $I_{\mathbf{n}}$ for transitions out of the ground vibrational state ψ_0 are evaluated using the matrix elements involving the precalculated vibrational wave functions $\psi_{\mathbf{n}}$ and the components $\mu_{y,z}$ of the dipole moment:

$$I_{\mathbf{n}} \sim E_{\mathbf{n}} [|\langle \psi_0 | \mu_y | \psi_{\mathbf{n}} \rangle|^2 + |\langle \psi_0 | \mu_z | \psi_{\mathbf{n}} \rangle|^2] . \quad (2)$$

Here $E_{\mathbf{n}}$ is the vibrational energy relative to the ground state. For C_{2v} symmetric isomers with the isotopic composition $^{12}\text{C}^{16}\text{O}_2$, only one of the two matrix elements in Eq. (2) is non-zero for a given \mathbf{n} . Indeed, the dipole moment function μ_y is of b_2 symmetry and promotes excitations to states with odd number of antisymmetric stretch quanta v_a ; the totally symmetric function μ_z mediates transitions to the complementary set of states with even v_a values.

The calculated IR spectra for the singlet bent isomers are shown in Fig. 2(d,e,f); the IR spectra of the triplet species are in Fig. 3(c,d). The intensities $I_{\mathbf{n}}$ are given relative to the intensity I_{010} of the fundamental bending excitation $(0, 1, 0)$. The IR spectra of all bent isomers are dominated by the transition to the antisymmetric stretch fundamental $(0, 0, 1)$. This can be explained by comparing the Herzberg-Teller expansion coefficients of different vibrational modes in Table I. The gradient $\partial\mu_y/\partial R_-$ of the dipole moment μ_y is noticeably larger than the gradients of μ_z with respect to α_{OCO} or R_+ . The relative intensities for the antisymmetric and symmetric stretch fundamentals I_{001}/I_{010} and I_{100}/I_{010}

are also listed in Table I. For $\text{CO}_2(72^\circ|\tilde{X}^1A')$, the intensity $I_{001}/I_{010} \sim 9$ is the smallest; it is close to the experimental value of 12 for the linear isomer $\text{CO}_2(180^\circ|X^1A')$.³³ For all other isomers in Table I, this intensity is noticeably larger and is either comparable to the value of $I_{001}/I_{010} = 28$ predicted³⁴ for the anion radical CO_2^- or exceeds it. The largest intensity of $I_{001}/I_{010} = 107$ is found for the singlet isomer $\text{CO}_2(118^\circ|2^1A')$. The different relative intensities I_{001}/I_{010} calculated for different isomers are primarily due to the variations in the intensity of the bending fundamental, which in turn correlate with the Herzberg-Teller coefficients $\partial\mu_z/\partial\alpha_{\text{OCO}}$. The actual vibrational wave functions are anharmonic, and the correlation is often imperfect (see Table I). In all bent molecules, the symmetric stretch mode is IR active. However, the relative intensity is modest, $I_{100}/I_{010} \sim 1$, matching that predicted for CO_2^- .³⁴ The exception is $\text{CO}_2(72^\circ|\tilde{X}^1A')$ for which this line is rather intense, $I_{100}/I_{010} = 7$, and can be used as a spectral marker of dioxiranylidene.

Despite many common features, the IR intensity patterns form a unique signature of a given isomer. For $\text{CO}_2(72^\circ|X^1A')$, the IR peaks are resolved only within 2000 cm^{-1} above the ground state [Fig. 2(d)] — the coordinate dependences of the dipole moments are close to linear. The frequency window $1100\text{ cm}^{-1} - 1800\text{ cm}^{-1}$, often used for the assignment of bent isomers,³⁵ contains two excitations lying 226 cm^{-1} apart, the already mentioned intense line I_{100} and the second overtone of the antisymmetric stretch mode I_{002} , both promoted by the dipole moment μ_z .

The IR spectrum of $\text{CO}_2(118^\circ|2^1A')$ extends over the energy range of more than 4000 cm^{-1} [Fig. 2(e)]. The main transitions stem from the dipole moment μ_y and terminate on the vibrational states with one quantum of antisymmetric stretch $v_a = 1$. Clearly seen in the spectrum is the bending progression $(0, v_b, 1)$ with $v_b \leq 5$ and the intensity which gradually decreases with increasing v_b . The frequency window $1100\text{ cm}^{-1} - 1800\text{ cm}^{-1}$ contains only one line I_{011} ; it lies 566 cm^{-1} above I_{001} . The spectrum of the triplet incarnation of this isomer, $\text{CO}_2(119^\circ|1^3A')$, is in many respects similar. The bending progression, however, is short while the symmetric stretch excitations with $v_s = 1$ are clearly seen [Fig. 3(c)]. The frequency window $1100\text{ cm}^{-1} - 1800\text{ cm}^{-1}$ contains the stronger line I_{011} and a weak peak of I_{100} . The asymmetric stretch line I_{001} lies just a few cm^{-1} below this window.

Characteristic for IR spectrum of the singlet isomer $\text{CO}_2(127^\circ|1^1A'')$ are excitations of the antisymmetric stretch overtones with $v_a = 1, 3$, as well as an unusually long progression of the symmetric stretch excitations with $v_s \leq 3$ [Fig. 2(f)]. Excitations, falling into the

frequency window $1100\text{ cm}^{-1} - 1800\text{ cm}^{-1}$, include two peaks, I_{100} and I_{011} , lying 293 cm^{-1} apart. The spectrum of the triplet isomer $\text{CO}_2(128^\circ|1^3A'')$ also includes transitions to states with $v_a = 1, 3$. The anharmonic couplings in this isomer are unusually strong, and several peaks in the vibrational spectrum are difficult to assign uniquely. The frequency window $1100\text{ cm}^{-1} - 1800\text{ cm}^{-1}$ includes a single assigned peak I_{101} lying $\sim 1000\text{ cm}^{-1}$ above I_{001} .

Shifts in the positions of the IR absorption lines upon isotope substitution often facilitate the experimental assignment, and isotope shifts in vibrational progressions are considered to be sensitive indicators of the isomer geometry. For example for CO_2^- , the measured isotope shifts were used to estimate the equilibrium angle of the radical.^{36,37} In this work, the isotope shifts are calculated for the singlet isotopomers, two of which are C_{2v} symmetric, $^{13}\text{C}^{16}\text{O}_2$ and $^{12}\text{C}^{18}\text{O}_2$, and one has the lower C_s symmetry, $^{16}\text{O}^{12}\text{C}^{18}\text{O}$. They are abbreviated as 636, 828, and 628, respectively; in the first, the central carbon atom is substituted, while in the other two the end oxygen atoms are substituted. Their IR spectra are calculated as described in Appendix, and the isotope shifts are found by matching states with the same vibrational assignments. The largest isotope shifts are found for the bending states $(0, v_b, 0)$ and the antisymmetric stretch states $(0, 0, v_a)$. They are shown in Fig. 4. Different bent isomers are marked with different colors, and different isotope combinations are marked with different symbols; the vibrational states are depicted regardless of their IR intensity. Common to most calculated isotope shifts is their near linear growth inside progressions with increasing vibrational energy. This indicates that the progressions are approximately harmonic. Indeed, for a harmonic oscillator the dependence of the isotope shift δG on the vibrational quantum number v_n (or the vibrational energy ϵ_n) is given by

$$\delta G(v_n) = \left(1 - \frac{\omega_n^i}{\omega_n^0}\right) \hbar\omega_n^0(v_n + 1/2) \equiv (1 - \rho_n)\epsilon_n \quad (3)$$

with the slope determined by the ratio ρ_n of the harmonic frequencies in the unsubstituted (ω_n^0) and substituted (ω_n^i) molecules. Dashed lines in Fig. 4 depict the corresponding predictions for each progression and each isotopomer.

For the bending progression (left panel), the harmonic prediction is rather accurate. The largest shifts are observed in the 828 isotopomer, while 636 gives the lower bound. As expected, the bending progression is characterized by large oxygen and small carbon isotope shifts. Note that for a given isotopomer, the symbols corresponding to different bent equilibria (and therefore differently colored) cluster around one straight line: The

isotope shifts in the bending progression are not sensitive to the equilibrium α_{OCO} angle and are similar for all bent isomers.

The isotope shifts in the antisymmetric stretch progression follow a different pattern (right panel). The smallest shifts are in the 828 isotopomer, and the largest shifts are found for 636, indicating that this progression responds stronger to the carbon substitution. The harmonic approximation appears accurate only for the open isomers $\text{CO}_2(118^\circ|2^1A')$ and $\text{CO}_2(127^\circ|1^1A'')$ (red and green symbols). For the cyclic isomer $\text{CO}_2(72^\circ|X^1A')$ (blue symbols), the deviations from the predictions of Eq. (3) are strong. For example in the cyclic 636 isomer, the slope of the dependence δG vs. ϵ_n is smaller than the prediction by a factor or two. In the cyclic 828 and 628 molecules, the actual slopes are larger than predicted. As a result, the isotope shift in the oxygen substituted cyclic 828 isotopomer is larger than in the carbon substituted cyclic 636 isotopomer, contrary to the expectations. Thus, the isotope shifts in the antisymmetric stretch progression $(0, 0, \nu_a)$ allow one to discriminate between the dioxiranylidene structure $\text{CO}_2(72^\circ|X^1A')$ and the open configurations $\text{CO}_2(118^\circ|2^1A')/\text{CO}_2(127^\circ|1^1A'')$.

IV. CONCLUSIONS AND OUTLOOK

This paper analyzes the properties of the activated neutral carbon dioxide molecules $\text{CO}_2(72^\circ|\tilde{X}^1A')$, $\text{CO}_2(118^\circ|2^1A')$, $\text{CO}_2(119^\circ|1^3A')$, $\text{CO}_2(127^\circ|1^1A'')$, and $\text{CO}_2(128^\circ|1^3A'')$. Their IR spectra are calculated using the new ab initio potential energy and electric dipole moment surfaces of the bent triplet states $1^3A'$ and $1^3A''$, as well as the previously reported (and improved) surfaces for the bent singlet states $2^1A'$ and $1^1A''$ and for the local dioxiranylidene minimum of the ground electronic state \tilde{X}^1A' . The main results can be summarized as follows:

1. The antisymmetric stretch fundamental $(0, 0, 1)$ is the strongest transition out of the ground vibrational state for all bent isomers. The intensity of this transition, I_{001}/I_{010} , measured relative to the intensity of the bending fundamental, is much larger than in linear CO_2 for all bent molecules but the triplet isomer $\text{CO}_2(128^\circ|1^3A'')$.
2. Individual isomers can be distinguished on the basis of their strong IR bands in the broad frequency interval, shown in Figs. 2 and 3, as well as in the narrow frequency

window $1100\text{ cm}^{-1} - 1800\text{ cm}^{-1}$. A unique feature of the cyclic isomer $\text{CO}_2(72^\circ|\tilde{X}^1A')$ in this window is a strong excitation of the symmetric stretch fundamental.

3. Isotope shifts, calculated for three singlet isotopomers, can be used as fingerprints of activated neutral CO_2 molecules. The shifts grow in the pure bending and antisymmetric stretch progressions, reaching $\geq 40\text{ cm}^{-1}$ already for the second pure overtones. For the cyclic CO_2 , the calculated isotope shifts strongly deviate from the nearly harmonic shifts predicted for other bent isomers.

The bent neutral isomers in the gas phase are generated via an electronic excitation across the large HOMO-LUMO gap. This requires the energy of at least 4.5 eV (for the triplet state) or 5.4 eV (for the singlet state) to be supplied by the incident light; the corresponding wavelengths are 274 nm and 230 nm, respectively. One way to reduce the excitation energy is to heat CO_2 gas and to irradiate vibrationally excited parent molecules.^{9,10,12} Temperatures over 2500 K are needed to substantially shift the optical absorption to wavelengths larger than 250 nm.^{9,10,12}

The gas phase data discussed in this paper can be useful in exploring and designing alternative routes to activate neutral CO_2 . Table I demonstrates that all bent isomers are polar molecules with permanent dipole moments. This suggests that the spectroscopy of CO_2 is sensitive to the environment effects. For example, interaction with a metal surface lowers the energy of a dipole, so that the optical excitation gap from the nonpolar linear ground electronic state into polar bent states becomes a function of the metal—molecule distance. The simplest estimate of this dependence is provided by classical electrostatics. The change in the energy E^* of a polar excited state due to the interaction of a classical dipole μ with its image in a perfect metal surface is given by³⁸

$$E^*(z) = E_\infty^* - \frac{\mu^2}{8(z - z_{\text{im}})^3}. \quad (4)$$

Here E_∞^* is the gas phase energy of the bent excited state relative to the nonpolar ground electronic state; z is the distance from the center of mass of CO_2 to the metal image plane located at z_{im} ; the dipole is assumed to lie perpendicular to the metal surface (carbon-down arrangement). CO_2 physisorbs on most metals,⁷ and the Eq. (4) is applied to Cu(100) for which the image plane is located at $z_{\text{im}} = 2.3 a_0$ in front of the last Cu plane.³⁹ Figure 5 shows the distance dependent excitation energies for $\text{CO}_2(118^\circ|1^1A')$ with the dipole moment

of $\mu = 0.99$ D and for $\text{CO}_2(119^\circ|1^3A')$ with the dipole moment of $\mu = 0.46$ D. The influence of the image potential is appreciable, and 1 bohr away from the image plane, i.e. $3.5 a_0$ away from the metal surface, the original excitation energy of the singlet state is decreased by almost 1 eV. A comparable reduction in the excitation energy can be achieved in the homogeneous gas phase only at temperatures over 7000 K. For the triplet state with smaller dipole moment, the excitation energy shifts by about 0.25 eV. Incidentally, these red shifts imply that the polar states stabilize relative to the dissociation thresholds because carbon monoxide $\text{CO}(\tilde{X}^1\Sigma^+)$ has a very small equilibrium electric dipole and is not affected by image forces.

Although the electrostatic effects are expected to be substantial at distances over $3 a_0$ from a metal surface,^{40,41} the actual CO_2/metal interaction is complicated, and the above estimate serves only for orientation. Interaction with metal surface significantly affects the electronic structure of the adsorbate molecule. Even in the simple model of Fig. 5, the singlet and the triplet states are seen to cross at distances $z - z_{\text{im}} < 0.9 a_0$. Quantum chemical calculations are therefore mandatory for a quantitative analysis of the optical excitation gap at different absorption sites and the degree of spin quenching in the electronically excited states near a metal surface. First principles calculations of the molecular excited electronic states near metal surfaces is a challenging problem,⁴² and this is the direction in which this study will be extended. The planned calculations will also allow one to address questions, related to the kinetics of the excited states, and to estimate the characteristic rates of electron transfer into metal, the rates of radiationless relaxation into the ground electronic state, and to compare them with the desorption rates of electronically excited CO_2 .

Appendix A: Quantum mechanical calculations of the vibrational spectra

Bound vibrational states in the potential wells of the bent singlet and triplet isomers are found by applying Filter Diagonalization⁴³ to the respective Hamiltonians set in the Jacobi coordinates R , r , and γ . Here R is the distance between the carbon atom and the center of mass of two oxygen atoms, r is the O–O distance, and γ is the angle between the vectors \mathbf{R} and \mathbf{r} . The calculations are performed using the expansion of the propagator in terms of Chebyshev polynomials, as implemented in the program package ‘PolyWave’.³¹ The settings for the iterative scheme are described in Refs. 2 and 12. The coordinate discrete

variable representation (DVR) grids in the calculations are as follows. For $\text{CO}_2(72^\circ|\tilde{X}^1A')$: 160 potential optimized DVR points in R and r , and 200 Gauss-Legendre DVR points in γ . For all other bent isomers: 70 and 110 potential optimized DVR points in R and r , respectively, and 100 Gauss-Legendre DVR points in γ . The assigned vibrational states for all isomers with the isotopic composition $^{12}\text{C}^{16}\text{O}_2$ are given in Table II. The same settings are used in the calculations of the vibrational states in the isotopically substituted carbon dioxide.

Acknowledgments

Financial support by the Deutsche Forschungsgemeinschaft is gratefully acknowledged.

-
- ¹ K. Yoshino, J. R. Esmond, Y. Sun, W. H. Parkinson, K. Ito and T. Matsui, *J. Quant. Spect. Radiat. Transf.* **55**, 53 (1996).
 - ² S. Yu. Grebenshchikov, *J. Chem. Phys.* **138**, 224107 (2013).
 - ³ C. Cossart-Magos, F. Launay and J. E. Parkin, *Mol. Phys.* **75**, 835 (1992).
 - ⁴ S. Wang, Z. Ding and X. Wang, *Chem. Commun.* **51**, 1517–1519 (2015).
 - ⁵ R. Kuriki, K. Sekizawa, O. Ishitani and K. Maeda, *Angew. Chem. Int. Ed.* **54**, 1–5 (2015).
 - ⁶ H.-J. Freund and R. P. Messmer, *Surf. Sci.* **172**, 1 (1986).
 - ⁷ U. Burghaus, *Prog. Surf. Sci.* **89**, 161 (2014).
 - ⁸ A. J. Traynor and R. J. Jensen, *Ind. Eng. Chem. Res.* **41**, 1935 (2002).
 - ⁹ S. C. Roy, O. K. Varghese, M. Paulose and C. A. Grimes, *ACSNano* **4**, 1259 (2010).
 - ¹⁰ M. A. Oehlschlaeger, D. F. Davidson, J. B. Jeffries and R. K. Hanson, *Chem. Phys. Lett.* **399**, 490 (2004).
 - ¹¹ O. Venot, N. Fray, Y. Benilan, M.-C. Gazeau, E. Hebrard, G. Larcher, M. Schwell, M. Dobrijevic and F. Selsis, *Astronomy & Astrophysics* **551**, A131 (2013).
 - ¹² S. Yu. Grebenshchikov, *J. CO2 Utilization* **15**, 32 (2016).
 - ¹³ G. J. van Rooij, D. C. M. van den Bekerom, N. den Harder, T. Minea, G. Berden, W. A. Bongers, R. Engeln, M. F. Graswinckel, E. Zoethout and M. C. M. van de Sanden, *Faraday Discuss.* **183**, 233 (2015).

- ¹⁴ A. Bogaerts, T. Kozák, K. van Laer and R. Snoeckx, *Faraday Discuss.* **183**, 217 (2015).
- ¹⁵ D. Mei, X. Zhu, C. Wu, B. Ashford, P. T. Williams and X. Tu, *Appl. Catal. B* **182**, 525 (2016).
- ¹⁶ A. Spielfiedel, N. Feautrier, C. Cossart-Magos, G. Chambaud, P. Rosmus, H.-J. Werner and P. Botschwina, *J. Chem. Phys.* **97**, 8382 (1992).
- ¹⁷ R. J. Buenker, M. Honigmann, H.-P. Liebermann and M. Kimura, *J. Chem. Phys.* **113**, 1046 (2000).
- ¹⁸ R. N. Dixon, *Proc. Roy. Soc. A* **275**, 431 (1963).
- ¹⁹ S. Yu. Grebenshchikov, *J. Chem. Phys.* **138**, 224106 (2013).
- ²⁰ J. Schmidt, M. S. Johnson and R. Schinke, *Proc. Natl. Acad. Sci. USA* **110**, 17691 (2014).
- ²¹ D. Picconi and S. Yu. Grebenshchikov, *Chem. Phys.* **481**, 231 (2016).
- ²² D. Feller and J. Katriel and E. R. Davidson, *J. Chem. Phys.* **73**, 4517 (1980).
- ²³ S. S. Xantheas and K. Ruedenberg, *Int. J. Quant. Chem.* **49**, 409 (1994).
- ²⁴ D.-Y. Hwang and A. Mebel, *Chem. Phys.* **256**, 169 (2000).
- ²⁵ T. H. Dunning, *J. Chem. Phys.* **90**, 1007 (1989).
- ²⁶ H.-J. Werner, P. J. Knowles, R. Lindh et al. *Molpro*, a package of ab initio programs, (2009). see <http://www.molpro.net>.
- ²⁷ S. Adachi, M. Sato, T. Suzuki and S. Yu. Grebenshchikov, *Phys. Rev. A* **95**, 033422 (2017).
- ²⁸ The C_{2v} symmetric barrier at $\alpha_{\text{OCO}} = 90^\circ$ and the CO bond distances $R_1 = R_2 = 2.46 a_0$ is not the true transition state for the carbon dioxide-to-dioxiranylidene isomerization; the true transition state is located at a distorted geometry of $\alpha_{\text{OCO}} = 91^\circ$, $R_1 = 2.33 a_0$ and $R_2 = 2.61 a_0$. This geometry is in good agreement with the earlier predictions of Ref. 23 ($\alpha_{\text{OCO}} = 92^\circ$, $R_1 = 2.33 a_0$ and $R_2 = 2.66 a_0$) as well as of Ref. 44 ($\alpha_{\text{OCO}} = 91.8^\circ$, $R_1 = 2.31 a_0$ and $R_2 = 2.60 a_0$). Xantheas and Ruedenberg²³ attributed the distortion of the transition state into C_s geometries to an intersection between the electronic states $1, 2^1A'$.
- ²⁹ J. F. Harrison, *J. Phys. Chem. A* **110**, 10848 (2008).
- ³⁰ P. R. Bunker and P. Jensen. *Molecular Symmetry and Spectroscopy*. NRC Research Press, Ottawa, (2006).
- ³¹ ‘PolyWave’ is a package of FORTRAN90 programs for iterative quantum mechanical calculations of bound states, dissociative resonance states, photoabsorption or photoemission spectra, as well as product state distributions in molecules with up to six internal degrees of freedom and many coupled electronic states. The package is available from S.Yu.G. upon request. .

- ³² E. Fermi, *Z. Phys.* **71**, 250 (1931).
- ³³ L. S. Rothman and L. D. G. Young, *J. Quant. Spectrosc. Radiat. Transfer* **25**, 505–524 (1981).
- ³⁴ M. Zhou and L. Andrews, *J. Chem. Phys.* **110**, 2414 (1999).
- ³⁵ V. P. Indrakanti, J. D. Kubicki and H. H. Schobert, *Fuel Processing Technology* **92**, 805 (2011).
- ³⁶ M. Allavena, R. Rysnik, W. Whilte, V. Calder and D. E. Mann, *J. Chem. Phys.* **50**, 3399 (1969).
- ³⁷ D. W. Green and K. M. Ervin, *J. Mol. Spectrosc.* **88**, 51 (1981).
- ³⁸ S. Holmström and S. Holloway, *Surf. Sci.* **173**, L647 (1986).
- ³⁹ A. G. Borisov, J. P. Gauyacq, A. K. Kazansky, V. V. Chulkov, V. M. Silkin and P. M. Echenique, *Phys. Rev. Lett.* **86**, 488 (2001).
- ⁴⁰ A. M. Gabovich, M. S. Li, H. Szymczak and A. I. Voitenko, *Surf. Sci.* **606**, 510 (2012).
- ⁴¹ D. Fernandez-Torre, O. Kupiainen, P. Pyykkö and L. Halonen, *Chem. Phys. Lett.* **471**, 239 (2009).
- ⁴² T. Klüner, N. Govind, Y.A. Wang and E. A. Carter, *Phys. Rev. Lett.* **86**, 5954 (2001).
- ⁴³ V. A. Mandelshtam, T. P. Grozdanov and H. S. Taylor, *J. Chem. Phys.* **103**, 10074 (1995).
- ⁴⁴ B. C. Hathorn and R. A. Marcus, *J. Chem. Phys.* **113**, 9497 (2000).
- ⁴⁵ D. Schröder, C. A. Schalley, J. N. Harvey and H. Schwarz, *Int. J. Mass Spectr.* **185/186/187**, 25 (1999).
- ⁴⁶ K. O. Hartman and I. C. Hisatsune, *J. Chem. Phys.* **44**, 1913 (1966).
- ⁴⁷ G. L. Gutsev, R. J. Bartlett and R. N. Compton, *J. Chem. Phys.* **108**, 6756 (1998).

TABLE I: Properties of the bent neutral C_{2v} symmetric CO_2 isomers: Equilibrium bond length R_e ; the quantum mechanical fundamental vibrational frequencies (comparisons to other calculations and/or experimental values are given parenthetically where available); depth ΔE_{well} of the potential wells of the isomers; the dipole moments μ_{eq} at equilibrium geometries; the Herzberg-Teller coefficients $|\partial\mu_i/\partial q_n|$ for the components $\mu_{i=y,z}$ and the symmetry coordinates $q_n = R_+, \alpha_{\text{OCO}}$ and R_- ; the calculated intensities I_n of the transitions from $(0,0,0)$ state to the vibrational states $(1,0,0)$ and $(0,0,1)$ relative to the intensity I_{010} of the $(0,1,0)$ fundamental. The same properties are also shown for linear CO_2 and the CO_2^- anion radical where available.

Isomer	$\text{CO}_2(70^\circ X^1A')$	$\text{CO}_2(118^\circ 2^1A')$	$\text{CO}_2(119^\circ 1^3A')$	$\text{CO}_2(127^\circ 1^1A'')$	$\text{CO}_2(128^\circ 1^3A'')$	$\text{CO}_2^-(138^\circ 1^2A')$	$\text{CO}_2(180^\circ X^1A')$
R_e, a_0	2.51	2.36	2.36	2.37	2.37	2.33 [45]	2.20
ω_s, cm^{-1}	1495 (1480 [24])	1336 (1297 [16])	1378 (1322 [16])	1282 (1264 [16])	1088	650 [45]	1388
ω_b, cm^{-1}	666 (802 [24])	576 (593 [16])	602 (591 [16])	671 (671 [16])	651	1172 [45]	667
ω_a, cm^{-1}	683 (830 [24])	846 (758 [16])	1095 (812 [16])	904 (789 [16])	614	1657—1690 [34,45,46]	2349
$\Delta E_{\text{well}}, \text{eV}$	0.45 ^a	0.25 ^{bc}	1.2 ^b	0.15 ^{bc}	0.56 ^b	0.26 ^d	5.45 ^b
$\mu_{\text{eq}}, \text{D}$	-0.25	0.99	0.46	0.36	0.25	0.27 [47]	0.0
$ \partial\mu_z/\partial R_+ , \text{D}/a_0$	0.3	0.1	0.05	0.12	0.18		
$ \partial\mu_z/\partial\alpha , \text{D}/\text{rad}$	0.15	0.1	0.15	0.20	0.25		
$ \partial\mu_y/\partial R_- , \text{D}/a_0$	1.2	0.8	1.1	0.85	1.0		
I_{100}/I_{010}	7.0	1.0	0.8	1.4	1.1	1.9 [34]	0
I_{001}/I_{010}	30	107	49	22	9	28 [34]	12 [33]

^aRelative to the barrier towards linear OCO minimum.

^bRelative to the triplet dissociation threshold $\text{CO}(\tilde{X}^1\Sigma^+) + \text{O}(^3P)$.

^cThe well depth relative to the singlet dissociation threshold $\text{CO}(\tilde{X}^1\Sigma^+) + \text{O}(^1D)$ is $\sim 2 \text{eV}$.

^dRelative to the threshold $\text{CO}_2 + e$ [45].

TABLE II: Calculated vibrational energies (relative to the vibrational ground state, in cm^{-1}) for the bent singlet and triplet isomers of CO_2 .

No.	$(v_s, v_b, v_a)^a$	$\text{CO}_2(72^\circ \tilde{X}^1A')$	$\text{CO}_2(118^\circ 2^1A')$	$\text{CO}_2(119^\circ 1^3A')$	$\text{CO}_2(127^\circ 1^1A'')$	$\text{CO}_2(128^\circ 1^3A'')$
1	(0,0,0)	0.0	0.0	0.0	0.0	0.0
2	(0,1,0)	666.2	576.8	602.6	671.1	651.8
3	(0,0,1)	682.8	846.1	1095.1	904.7	614.7
4	(1,0,0)	1494.6	1336.1	1377.8	1282.0	1088.4
5	(0,2,0)	1362.6	1157.3	1205.5	1341.5	1302.0
6	(0,1,1)	1321.3	1404.4	1679.1	1559.5	1239.6
7	(0,0,2)	1268.6	1816.0	2189.9	1899.1	
8	(1,1,0)	2145.9	1905.0	1970.6	1947.9	1718.5
9	(0,3,0)	2041.7	1743.4	1809.4	2011.8	
10	(1,0,1)	2228.3	2114.6	2406.2	2127.3	1622.8
11	(0,2,1)	1956.9	1975.0	2263.1	2213.8	1861.9
12	(0,1,2)	1905.9	2370.2	2764.5	2537.3	
13	(2,0,0)		2655.3	2743.4	2560.2	
14	(1,2,0)		2480.7	2563.1	2612.2	
15	(0,4,0)		2333.7	2415.0	2682.3	
16	(1,1,1)		2670.4	2977.0	2771.7	2209.3
17	(0,3,1)		2550.6	2847.6	2867.4	2481.5
18	(0,0,3)	1866.8	2798.4	3283.8	2927.0	2632.7
19	(1,0,2)		3068.3	3441.6	3086.9	
20	(0,2,2)		2939.8	3342.8	3178.9	
21	(2,1,0)		3218.0	3317.9	3217.2	
22	(1,3,0)		3058.5	3155.4	3276.2	
23	(0,5,0)		2922.6	3022.3	3352.2	
24	(2,0,1)		3386.5	3715.1	3353.0	
25	(1,2,1)		3231.1	3547.5	3416.1	2797.8
26	(0,4,1)		3128.1	3433.1	3520.6	
27	(0,1,3)		3340.3		3559.0	
28	(1,1,2)		3617.5		3718.1	
29	(0,3,2)		3497.7		3820.7	
30	(3,0,0)		3958.5		3826.1	

TABLE II: *Continued from previous page*

No.	$(v_s, v_b, v_a)^a$	$\text{CO}_2(72^\circ \tilde{X}^1A')$	$\text{CO}_2(118^\circ 2^1A')$	$\text{CO}_2(119^\circ 1^3A')$	$\text{CO}_2(127^\circ 1^1A'')$	$\text{CO}_2(128^\circ 1^3A'')$
31	(2,2,0)		3786.7	3888.6	3872.7	
32	(1,4,0)			3746.9	3939.3	
33	(0,0,4)				3971.7	
34	(2,1,1)				3985.9	
35	(0,6,0)			3631.0	4021.4	
36	(1,3,1)				4058.3	
37	(1,0,3)				4065.4	
38	(0,5,1)			4019.2	4172.4	
39	(0,2,3)				4194.2	
40	(2,0,2)				4299.9	
41	(1,2,2)				4350.1	
42	(0,4,2)				4462.5	
43	(3,1,0)				4474.3	

^a v_s , v_b , and v_a are quantum numbers of the symmetric stretch, bend, and antisymmetric stretch vibrations.

FIG. 1: (a) Experimental absorption cross section of CO_2 ($T = 195 \text{ K}$) as a function of photon energy.¹ Thin sticks mark the major experimental peaks and their calculated counterparts (resonance positions). Theoretical electronic assignments of major spectral bands² are given in terms of equilibrium bending angles and main molecular motions (shown as cartoons). (b) Potential energy profiles along the minimum energy path shown as functions of the OCO bond angle for the ground electronic state (black), the two singlet states $2^1A'$ and $1^1A''$ (red) and the two triplet states $1^3A'$ and $1^3A''$ (blue). Dipole moment vectors are sketched to scale for each bent equilibrium. The drawings are ordered from left to right according to the equilibrium angle they illustrate. Dashed horizontal lines mark the positions of the dissociation thresholds $\text{CO}(\tilde{X}^1\Sigma^+) + \text{O}(^1D)$ (red; $D_0(\text{S})$) and $\text{CO}(\tilde{X}^1\Sigma^+) + \text{O}(^3P)$ (blue; $D_0(\text{T})$).

FIG. 2: Dipole moment surfaces and infrared spectra of singlet bent isomers $\text{CO}_2(70^\circ|X^1A')$ (a,d), $\text{CO}_2(118^\circ|2^1A')$ (b,e), and $\text{CO}_2(127^\circ|1^1A'')$ (c,f). In (a—c), the functions μ_y and μ_z are shown in the plane (R_1, R_2) , with the bending angle fixed at the respective equilibrium values. The antisymmetric component μ_y is shown above the diagonal. For μ_y , the dashed (dotted) contour corresponds to -0.10 D (-0.18 D) in (a) and (b), and 0.10 D (0.02 D) in (c). The symmetric component μ_z is shown below the diagonal. For μ_z , the dashed (dotted) contour corresponds to -0.22 D (-0.38 D) in (a); 1.07 D (0.99 D) in (b); and 0.51 D (0.42 D) in (c). Black dots indicate equilibrium bond distances. In (d—f), vibrational excitations via μ_y (μ_z) are shown with blue (red) sticks. Assignments of the main IR peaks in terms of three vibrational quantum numbers (v_s, v_b, v_a) are given. The IR intensities are normalized to the intensity of the bending fundamental $(0, 1, 0)$.

FIG. 3: Dipole moment surfaces and infrared spectra of bent isomers $\text{CO}_2(119^\circ|1^3A')$ (a,c), and $\text{CO}_2(128^\circ|1^3A'')$ (b,d). The layout is the same as in Fig. 2. For μ_y (above the diagonal), the dashed (dotted) contour corresponds to 0.26 D (0.18 D) in (a) and (b). For μ_z (below the diagonal), the dashed (dotted) contour corresponds to 0.51 D (0.42 D) in (a) and 0.26 D (0.18 D) in (b).

FIG. 4: Isotopic shifts relative to $^{12}\text{C}^{16}\text{O}_2$ in the bending (left panel) and the antisymmetric stretch (right panel) progressions of singlet bent isomers. Different colors distinguish different bent structures; different symbols distinguish different isotopic substitutions as indicated in the legends in the two panels. For $\text{CO}_2(118^\circ|2^1A')$, states belonging to the progression $(0, v_b, 1)$ are used.

FIG. 5: The dependence of the zero-point energies of the bent states $2^1A'$ (blue) and $1^3A'$ (red) on the distance to the image plane of Cu(100) as predicted by Eq. (4). Energies are measured relative to the zero-point vibrational state of CO₂ in the linear ground electronic state (horizontal dashed line). The image plane of Cu(100) (vertical dashed line) is located $2.3 a_0$ outside the last Cu plane.

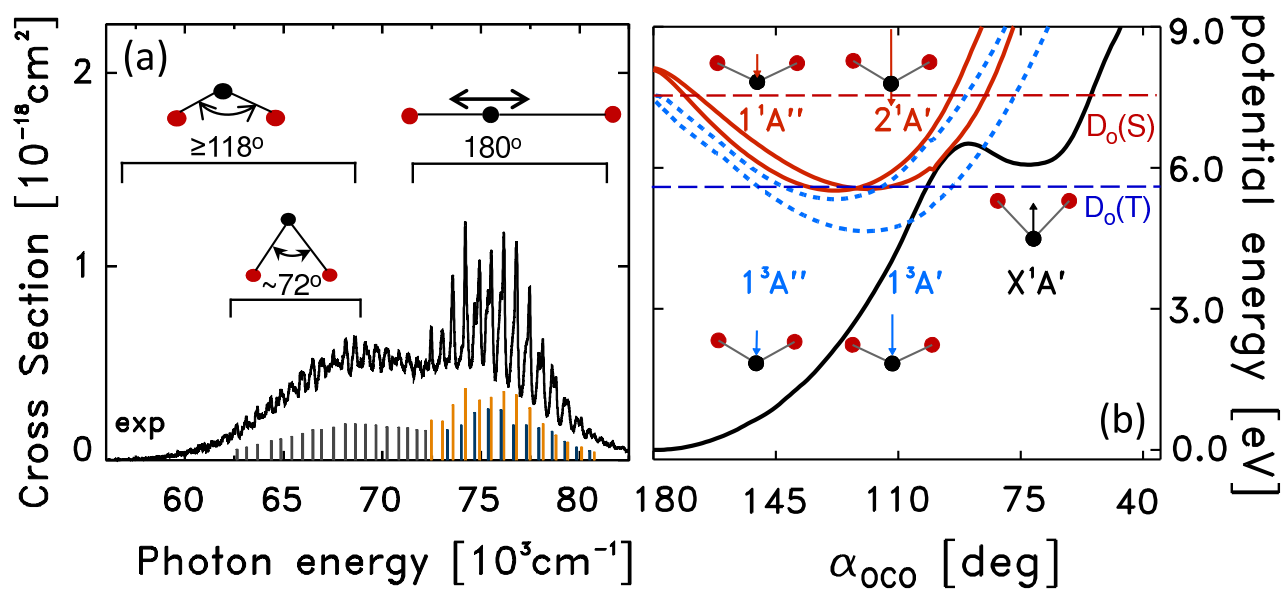


Fig. 1

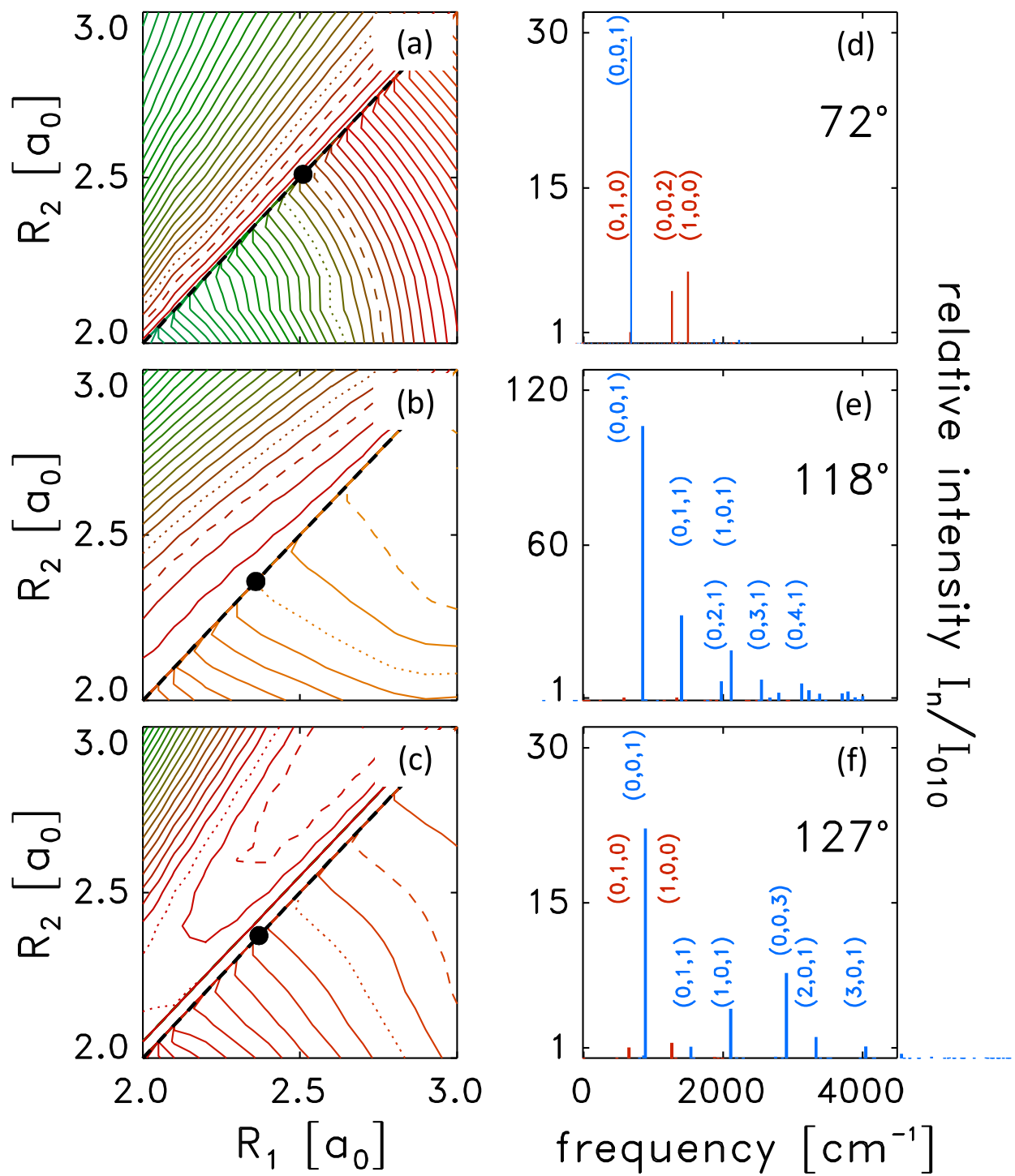


Fig. 2

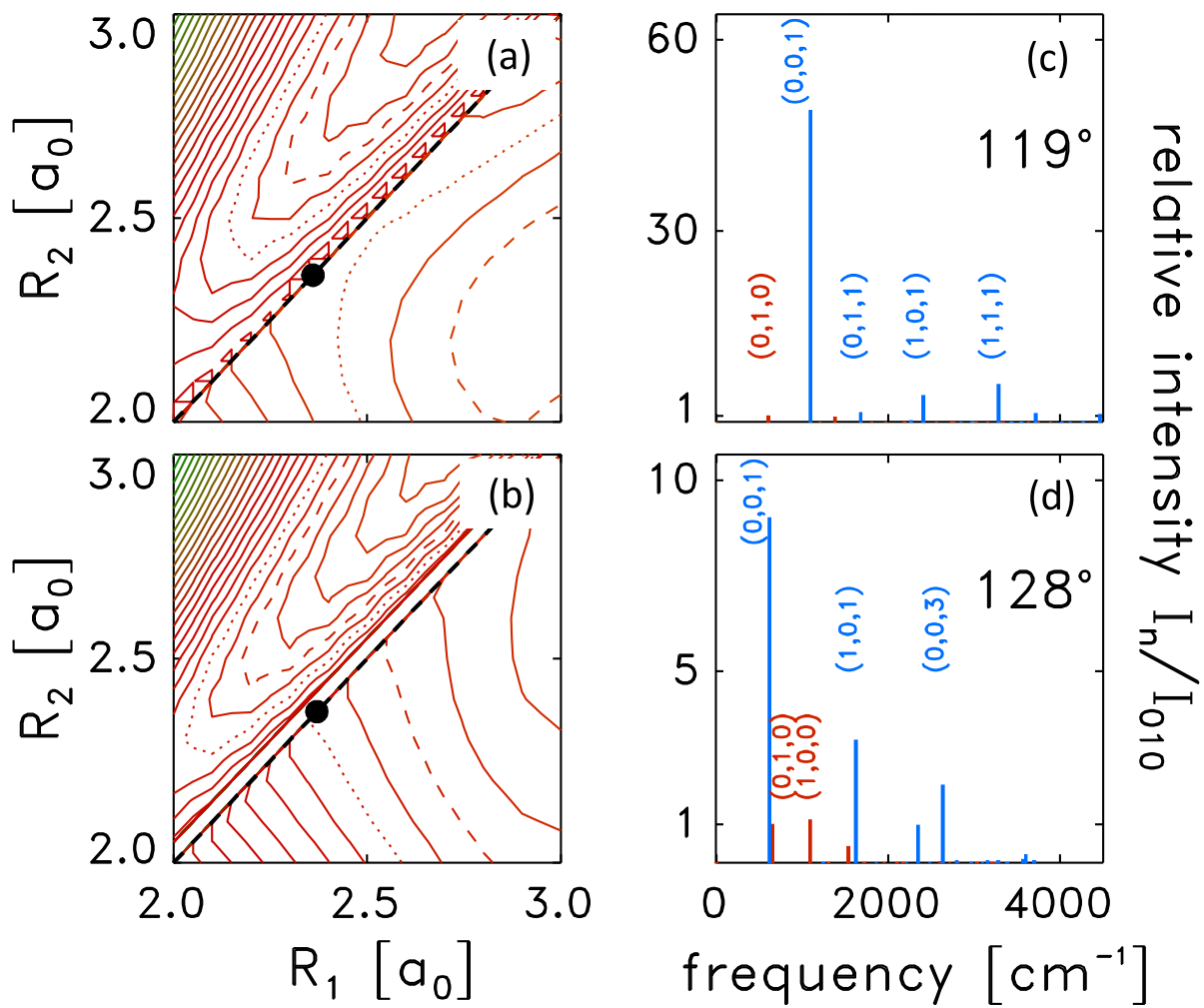


Fig. 3

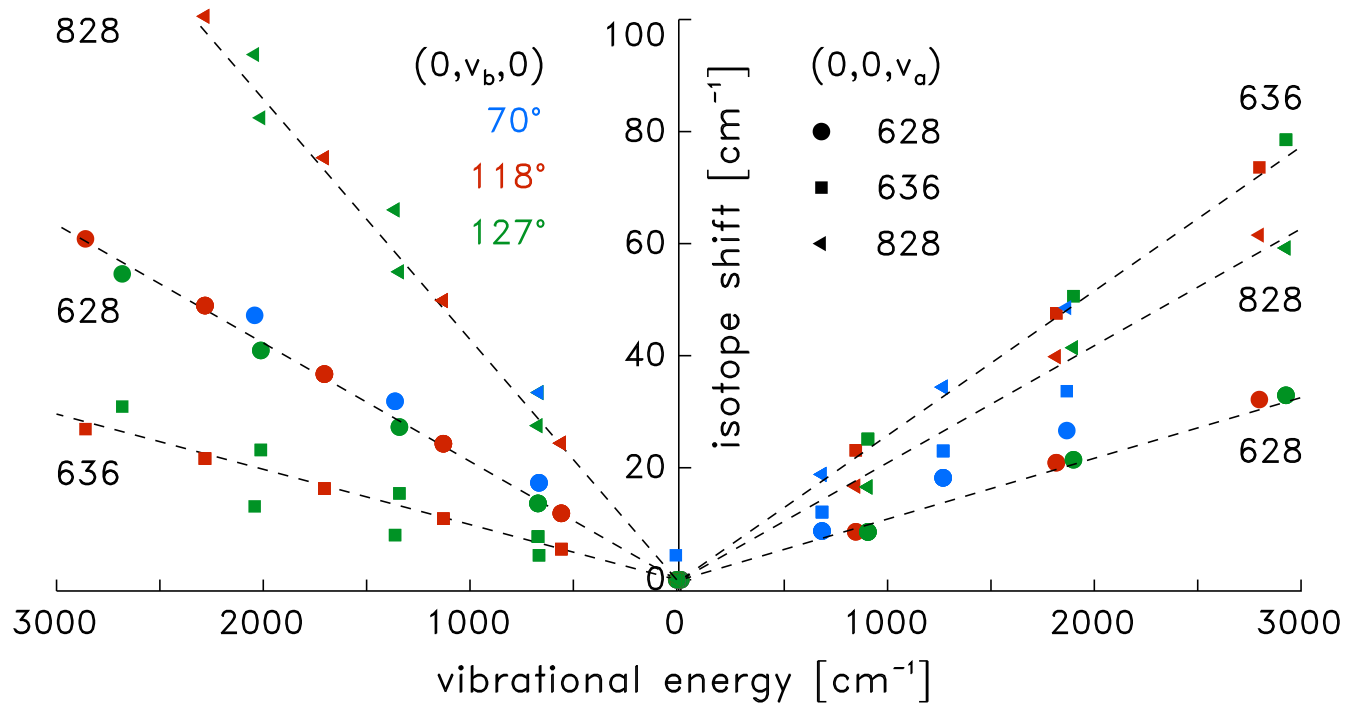


Fig. 4

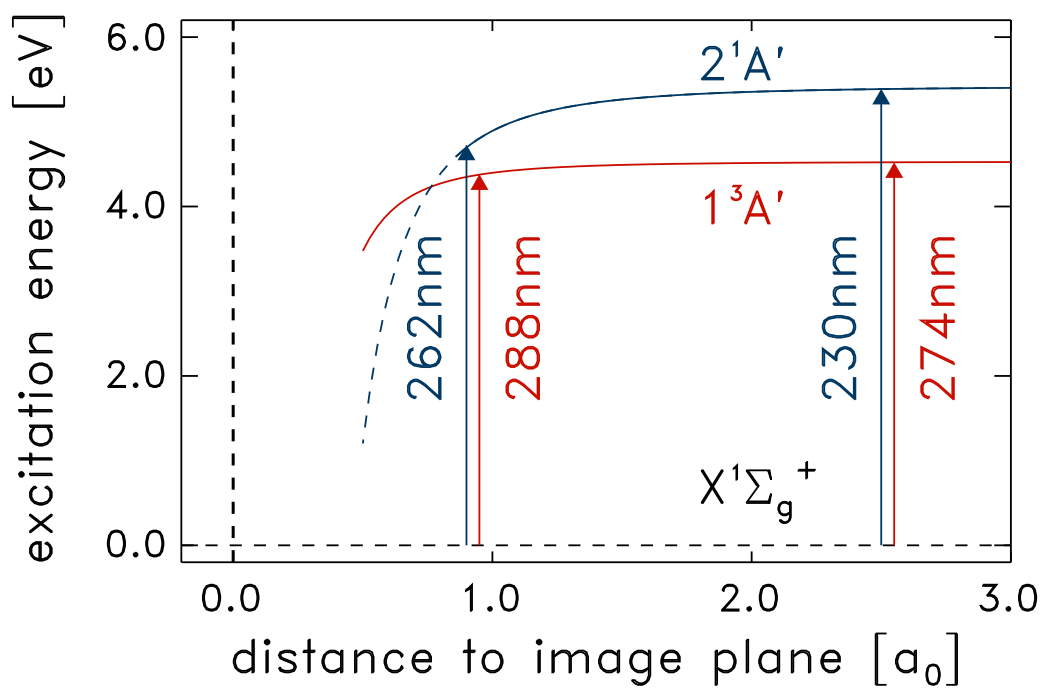


Fig. 5